IEEE *Access*

Multidisciplinary : Rapid Review : Open Access Journal

Industrial Grade Adaptive Control Scheme for a Micro-Grid Integrated Dual Active Bridge Driven Battery Storage System

NASIM ULLAH[ID][1], **ZAHEER FAROOQ**[ID][2], **IRFAN SAMI**[ID][3], **MD. SHAHARIAR CHOWDHURY**[4],
KUAANAN TECHATO[ID][4,5], **AND HEND IBRAHEEM ALKHAMMASH**[ID][1]

[1]Department of Electrical Engineering, College of Engineering, Taif University, P.O. Box 11099, Taif 21944, Saudi Arabia
[2]Department of Electrical Engineering, CECOS University of IT and Emerging Sciences, Peshawar 25000, Pakistan
[3]School of Electrical and Electronics Engineering, Chung-Ang University, Seoul 06974, South Korea
[4]Faculty of Environmental Management, Prince of Songkla University, Hat Yai 90112, Thailand
[5]Environmental Assessment and Technology for Hazardous Waste Management Research Center, Faculty of Environmental Management, Prince of Songkla University, Hat Yai 90112, Thailand

Corresponding author: Kuaanan Techato (kuaanan.t@psu.ac.th)

ABSTRACT In this paper, an industrial grade adaptive control scheme is proposed for a micro-grid integrated dual active bridge driven battery management system (DIBMS). A benchmark industrial grade adaptive control scheme depends on two factors namely robustness and computational resource utilization when such controllers are implemented over processors. The mathematical model of DIBMS system is nonlinear, thus for desired response, non-linear controllers based on sliding mode variable structure control theory suits it well for the state regulation problem of DIBMS, however such controllers utilize high computational resources when practically implemented over processors. Keeping in view the above performance indices, this paper proposes an industrial grade computationally efficient and finite time adaptive robust convergent control for DIBMS system. A proportional integral (PI) scheme is used as central control unit and Hebbian algorithm with double integration of the state error is introduced for online tuning the gains of central control unit. The robustness and computational resource efficiency of the proposed control paradigm is validated using a laboratory scale test bench through TI Launchpad (TMS320F28379D). The superiority of the proposed AI based PI control paradigm is compared with classical PI, integer order sliding mode control (SMC), and fractional order SMC (FOSMC) in terms of computational resource utilization and robustness under all test conditions.

INDEX TERMS DC micro-grid, fractional calculus, fractional control theory, industrial grade control, robust control, energy management, sliding mode control.

I. INTRODUCTION

In order to ensure the reliability and stability of the existent power grids, an innovative and modern technology namely smart grids is under the focus of the research community. This technology incorporates all measures to adopt clean energy resources such as solar and wind energy [1]–[3]. Solar and wind energy sources have intermittent nature, thus integration of such sources with the conventional grids may introduce issues like frequency and voltage instabilities. Thus in order to stabilize such grids, energy storage system is integrated to

The associate editor coordinating the review of this manuscript and approving it for publication was Sanjeevikumar Padmanaban[ID].

the micro-grid [3], [4]. In direct current (DC) micro-grids, the energy storage system is utilized to supply or draw energy from the DC bus depending on situations whether the source energy is in deficient or excess mode.

The integration of battery storage system requires a bidirectional DC-DC converter. Such converters are either galvanically isolated or non-isolated type. Non isolated converter requires auxiliary circuitry for safety, while the isolated type is composed of a high-frequency transformer for galvanic isolation between its stages [3], [4]. Dual Active Bridge (DAB) is the widely utilized converter for bidirectional power exchange with galvanic isolation. DAB offers advantages such as small component count wide range of

IEEE Access

N. Ullah *et al.*: Industrial Grade Adaptive Control Scheme for a Micro-Grid Integrated DAB Driven Battery Storage System

voltages operation [5], [6]. Several isolated bidirectional typologies have been reported, including two-device topologies such as dual fly-back converter, dual cuk converter and dual-zeta converter [7], [8], four-device topologies such as forward fly-back converter, dual-push-pull converter, push-pull forward converter, push-forward-fly-back converter, and dual-half-bridge converter [9], [10], and eight-device typologies such as dual-active-bridge (DAB) converter [11]. The isolated bidirectional converters, DAB has the lowest volume of filter and largest capacity of power transfer [12]. Such converters consist of two bridges namely low voltage (LV) and high voltage (HV) bridges.Single phase shift (SPS) modulation methods are reported for DIBMS in [13]–[15].

In order to control the DAB integrated battery storage system, modulation schemes of the converter play vital role. There are several modulation schemes such as single phase shift (SPS), double phase shift (DPS) and triple phase shift (TPS) modulation schemes.In SPS modulation method, two bridges are modulated using a square wave with a phase-shift angle ϕ and it can be leading or lagging depending on the mode of power flow [15].The efficiency of SPS method is low and to improve the power transfer efficiency of the DAB converters and to reduce stresses during high frequency switching, researchers reported dual phase shift (DPS) modulation scheme [16], [17].In order to further enhance the power transfer efficiency, triple mode phase shift (TPS) modulation scheme is reported in [18], [19]. TPS scheme has 3 degree of freedom to control, DPS requires two degree of freedom and SPS requires only one parameter.Apart from the modulation schemes, closed loop controllers play vital role to stabilize and achieve the desired performance of the DIBMS system. In the existent literature, several linear and nonlinear control methods have been reported for the subject application.

The traditional linear proportional, integral and derivative (PID) controllers have been widely applied in the existing literature [20]–[24]. In [20] the authors presented fixed gain PI controller for the regulation of DC bus voltage in DIBMS. A fixed gain PI controller is implemented for a laboratory scaled DIBMS system and presented in [21], [22]. Similarly the stability analysis of DC micro-grid is presented in [23], [24]. A PI controller is reported for DAB converter integrated with fuel cell applications [25]. Advanced versions of PI controller namely feed-forward PI, proportional-resonant PI, double loop PI and current sensor-less PI controllers have been reported in [26]–[29]. Applying linear controllers to DAB converted integrated systems may show poor performance, however at the same time an advantage of its utilization includes ease of practical implementation.

Among the nonlinear control schemes, sliding mode control (SMC) has been widely reported for renewable energy and power systems applications. SMC methods are reported in [30], [31] for DAB converter integrated battery storage system. A sliding mode control scheme based on an average output current model of a DAB converter has been reported in [32]. Classical SMC method has several disadvantages

such as high frequency chattering in control signal and limited switching on a hardware platform. In order to address the aforementioned problems, a double integral sliding mode control (DSMC) is proposed for battery energy storage systems in [30] and the validity was verified experimentally. In [33], a terminal sliding mode control is reported for compensation of perturbation.A sliding mode (SM)-based direct power control (DPC) scheme is proposed and verified experimentally for DAB converter application [34]. Similarly a proportional robust control based on sliding mode method is proposed in [35].

The application of intelligent control methods based on fuzzy logic system (FLC) and artificial neural network (ANN) to power systems have been widely reported in the literature [36], [37]. For energy storage applications utilizing DAB converters,a FLC based control is investigated in [37]. Similarly a PI based fuzzy controller (PIFC) has been reported in [38]. FLC based control schemes require user experience and it also increases computationally complexity when implemented over processors. An ANN based controller is proposed for power flow management of an electric vehicles and bidirectional DC-DC converters in [19] and [39] respectively. Apart from integer order control schemes, FOC is finding interesting applications in all fields of engineering and applied sciences. Fractional order sliding mode controllers have been proposed for renewable energy applications in [40], [41]. Similarly a fractional order PID control scheme is reported in [42] for a boost mode application of a boost converter. Similarly a non integer order fuzzy logic control (FO-FLC) system us analyzed for photo-voltaic (PV) system [43]. Fuel cell energy management is difficult due to the wide output voltage and high current, thus a fractional order PID controller is introduced in [44] for optimal management, while for switched mode power supply applications, a fractional order (FO) proportional integral (FOPI) controller is implemented and reported in [45].

Industrial grade feedback controllers must exhibit the following two important properties: **1.** *robustness against uncertainties* **2.** *computationally efficient.*In the above cited literature different linear, nonlinear and intelligent controllers have been discussed, however the implementation complexity of such controllers have rarely been reported in literature. In this regard several researchers reported some analysis such as computationally efficient fuzzy control [46], computationally efficient self-tuning controller for DC-DC switch mode power converters [47], computationally efficient predictive robot control [48],computationally efficient distributed predictive controller [49] and computational resource analysis over FPGA for fractional order control (FOSMC) scheme in [50].

Based on the above cited literature, the contributions of this paper are highlighted as follows:

1.*Micro-grid energy management and control requires multiple control loops and energy management algorithms. For practical implementations, the algorithms must be computationally efficient. This article proposes an industrial*

N. Ullah *et al.*: Industrial Grade Adaptive Control Scheme for a Micro-Grid Integrated DAB Driven Battery Storage System

IEEE *Access*

grade computationally efficient adaptive robust control scheme for micro-grid integrated DIBMS system

2.The robustness and computational efficiency of the proposed control system is compared with SMC, fractional order SMC (FOSMC) and classical PI controllers using hardware in the loop (HIL) and processor in the loop (PIL) experiments

Moreover, the paper organization is given as: The overall system and its configuration is described in section II. Section III gives the mathematical formulation of the proposed DIBMS system. The mathematical proof of all the discussed and proposed control paradigms is given in section IV, whereas the results and its discussion is done Section V. Finally the paper is concluded in Section VI.

II. SYSTEM DESCRIPTION

The micro-grid integrated DIBMS system block diagram is shown in Fig. 1. As shown in the block diagram, the micro-grid consists of renewable energy sources (RES-1, RES-2), converter driven load, and DAB integrated BMS system. The energy transfer between the battery storage and DC bus is done using a bi-directional DAB converter. This research work is focused on closed loop control system of DAB integrated BMS system so before formulating the control system, a detailed mathematical analysis is presented in the next section.
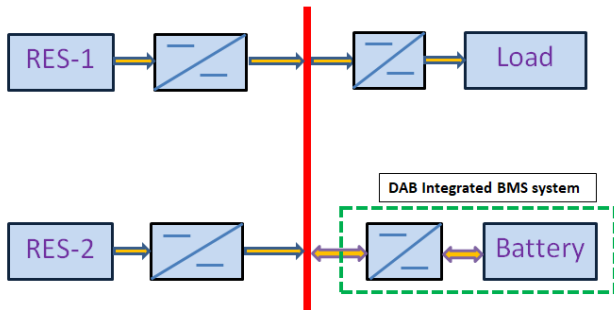

FIGURE 1. Block diagram of DAB integrated BMS.

III. MATHEMATICAL MODELING

A nonlinear state space model of DIBMS system is represented as follows [51]:

$$\dot{X} = \begin{bmatrix} \dfrac{-8}{C_{out}\pi^2} \displaystyle\sum_{n=1,3,5,...}^{\infty} \dfrac{cos\,(\varphi_z\,(n))}{n^2\,|Z\,(n)|} V_{load} & 0 \\ 0 & 0 \end{bmatrix} X$$

$$+ \begin{bmatrix} \dfrac{8}{C_{out}\pi^2} \displaystyle\sum_{n=1,3,5,...}^{\infty} \dfrac{1}{n^2\,|Z\,(n)|} N V_{source} \\ 0 \end{bmatrix} U + D(t) \quad (1)$$

From (1), the matrices and disturbance term $D(t)$ are represented as follows:

$$A(X) = \begin{bmatrix} \dfrac{-8}{C_{out}\pi^2} \displaystyle\sum_{n=1,3,5,...}^{\infty} \dfrac{cos\,(\varphi_z\,(n))}{n^2\,|Z\,(n)|} V_{load} & 0 \\ 0 & 0 \end{bmatrix}$$

$$B(X) = \begin{bmatrix} \dfrac{8}{C_{out}\pi^2} \displaystyle\sum_{n=1,3,5,...}^{\infty} \dfrac{1}{n^2\,|Z\,(n)|} N V_{source} \\ 0 \end{bmatrix};$$

$$D(t) = -\dfrac{i_{load}}{C_{out}}$$

The state X represents the voltage dynamics of DIBMS system. Any perturbation will lead to an uncertainty in the matrices i.e. $\Delta A(X)$ and $\Delta B(X)$, therefore the lumped disturbance term $G(t)$ is expressed as follows:

$$G(t) = D(t) + \Delta d_{load} + \Delta d_{source} + \Delta A(X) + \Delta B(X) \quad (2)$$

In (2), the source and load side disturbances are represented as Δd_{source} and Δd_{load} respectively. (1) is expressed as follows:

$$\dot{X} = A(X) + B(X)U + G(t) \quad (3)$$

Assumption 1: The following inequality is assumed to be valid for the lumped uncertainty term $G(t)$

$$||G(t)|| \leq \sigma_1 \quad (4)$$

Assumption 2: The constant $\Omega(S_{vFO})$ utilized in the stability proof of the FOC's is assumed to be upper bounded such that the following expression is true: $\Omega(S_{vFO}) \leq \chi_1$

Where χ_1 represents a known constant. The voltage error is defined as follows:

$$e = X - X_d \quad (5)$$

where X represents the feedback voltage while X_d is the reference command.

IV. CONTROL SYSTEM FORMULATION

This section is focused on formulation of the proposed control system. To have a fair robustness comparison and computational resources, robust control system namely sliding mode control (SMC) and FOSMC controllers are also formulated in the next subsections.

A. PROPOSED ADAPTIVE PI CONTROL

In this section a computationally efficient finite time adaptive robust PI control system is formulated for the DIBMS system. A PI control paradigm is utilized to stable the system nominal dynamics, while the adaptive part of the control system based on ANN is used to adaptively adjust the weights of the ANN controller. The total control effort is the sum of the PI and adaptive ANN controllers. A block diagram of the proposed control system is shown in Fig. 2. SPS modulation technique is used to drive the power switches of LV bridge ($S_1 - S_4$) and HV bridge ($S_5 - S_8$). As shown in Fig. 2, there are two control loops working in parallel. A fixed gain PI control scheme is used to achieve the stable nominal dynamics of (3) while the adaptive ANN controller compensates the nonlinear dynamics including the parametric uncertainty and disturbances of (3). Double integral of error based hebbian learning algorithm is used to adjust the weights of the ANN
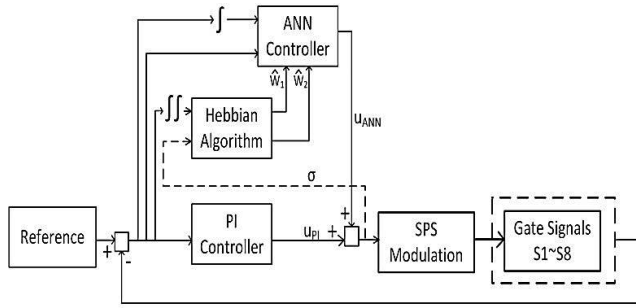
IEEE *Access*

N. Ullah *et al.*: Industrial Grade Adaptive Control Scheme for a Micro-Grid Integrated DAB Driven Battery Storage System

FIGURE 2. Block diagram of industrial grade adaptive PI control.

controller online in finite time. Thus the total control effort is expressed as follows:

$$U = U_{PI} + U_{ANN} \qquad (6)$$

From (6), the discrete PI control system is expressed as follows:

$$U_{PI}(n) = W_1 e(1) + W_2 \sum_{n=1}^{k} e(n) \qquad (7)$$

Here W_1 and W_2 represent the proportional and integral gains respectively. Note that W_1 and W_2 are fixed gains to be tabulated later. PI controller is discretized using Tustin method. ANN control system is shown as follows:

$$U_{ANN}(n) = \sum_{m=1}^{k} \widetilde{W}_m(n) E_m(n) \qquad (8)$$

(8) represents a single neuron ANN controller with two inputs and adjustable weights. For $m = 1, 2$, the adjustable weights are expressed as $\widetilde{W}_1$ and $\widetilde{W}_2$. Moreover for $m = 1, 2$, the term $E_1(n) = e(n)$ represents the voltage error and $E_2(n) = \sum_{i=1}^{k} e(i)$ shows the integral of the error $e(n)$. From (6), (7) and (8), the total control effort is expressed as follows:

$$U(n) = (W_1 + \widetilde{W}_1)e(1) + (W_2 + \widetilde{W}_2) \sum_{n=2}^{k} e(n) \qquad (9)$$

The adaptive tuning of weights $\widetilde{W}_i$ is done using double integral of error based hebbian algorithm which is shown as follows:

$$\widetilde{W}_i(n) = \widetilde{W}_i(n-1) + \eta_i Z_i(n) U(n) \qquad (10)$$

In (10), $Z_i(n) = \sum_{n=1}^{k} \sum_{n=1}^{k} e(n)$ that shows the discrete double integrator of the error $e(n)$, $U(n)$ represents the control signal at n^{th} sample and η_i represents the learning rates.

Remark IV-A: Equation (10) is implemented using discontinuous projector operator shown as follows:

$$\widetilde{W}_i(n) = proj_{\widetilde{W}_i(n)}[\zeta \widetilde{W}_i(n)] \qquad (11)$$

where ζ represents the learning gain. The projection operator is defined as follows:

$$proj_{\widetilde{W}_i(n)}(\star) = \begin{bmatrix} 0 & if\ \widetilde{W}_i(n) = W_i(n)_{max}\ and\ \star > 0 \\ 0 & if\ \widetilde{W}_i(n) = W_i(n)_{min}\ and\ \star < 0 \\ \star & otherwise \end{bmatrix} \qquad (12)$$
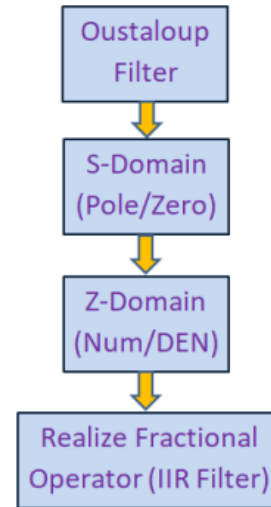
FIGURE 3. Implementation of fractional operator.

TABLE 1. System parameters.

Parameters	Value
Rated power	150 Watts
Input voltage v_{source}	12 to 16 V
Output voltage v_{out}	20 to 24 V
f_s	200Khz
C_{in}, C_{out}	100uF, 200uF
Transformer,s turn ration	1:2
Leakage inductance(L_k)	50uH
Variable load	50-300 watts

TABLE 2. Control system parameters.

Controller	Parameters	Value
Adaptive PI	W_1	1.5
	W_2	1.2
	η_1	1^{-8}
	η_2	1.25^{-8}
Integral SMC	C_1	1.5
	C_2	1.2
	k_v	0.5
FOSMC	α	$0.99, 0.95$
	C_3	1.5
	C_4	1.2
	k_{v1}	0.5
	w_b, wh	0,500Hz

B. INTEGER ORDER SLIDING MODE CONTROL

In this subsection, integer order SMC is formulated for DIBMS system. The sliding surface is defined as follows:
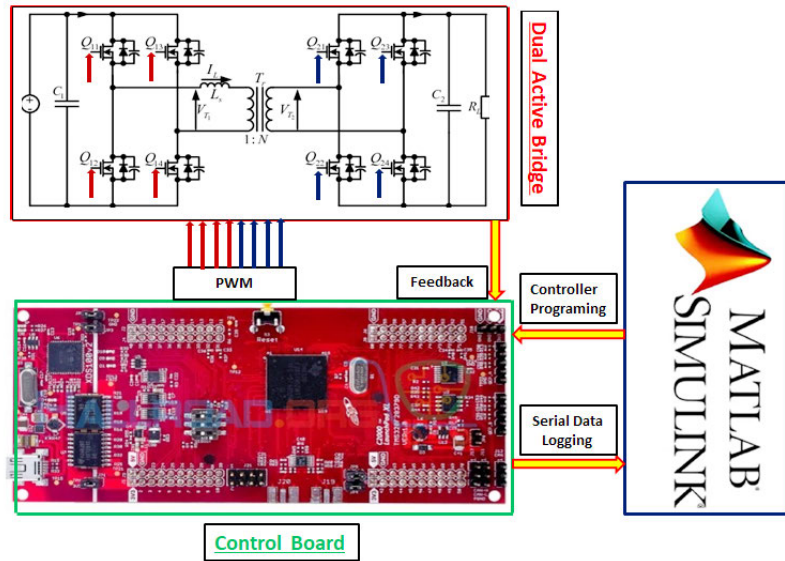
$$S_{vIO} = C_1 e + C_2 \int e \qquad (13)$$

N. Ullah *et al.*: Industrial Grade Adaptive Control Scheme for a Micro-Grid Integrated DAB Driven Battery Storage System

IEEE *Access*

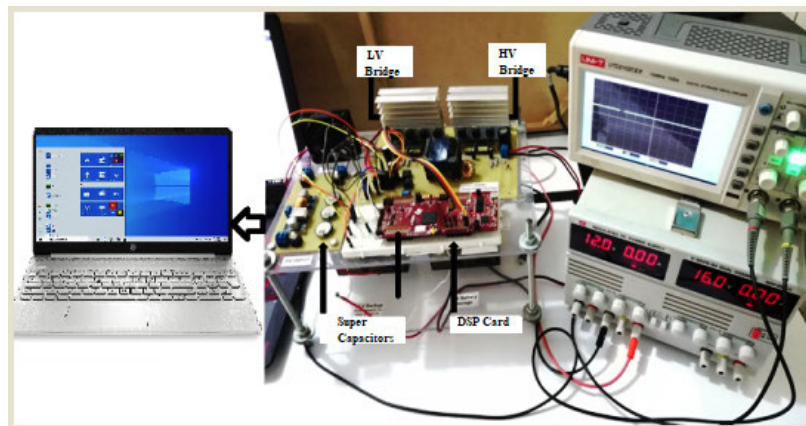**FIGURE 4.** Block diagram of HIL testing.

FIGURE 5. HIL testing.

where e is already defined in (5). Moreover C_1 and C_2 represent sliding surface constants. Differentiating (13) and by combining it with (3), the following expression is obtained:

$$\dot{S}_{vIO} = C_1[A(X) + B(X)U + G(t) - \dot{X}_d] + C_2e \quad (14)$$

From (14), the control law is derived as follows:

$$U = (C_1B(X))^{-1}[-C_1A(X) - C_2e + C_1\dot{X}_d - k_v sgnS_{vIO}] \quad (15)$$

Theorem 1: There exists a scalar function V_{IO} with continuous first derivative such that [52]:

1. *V_{IO} is positive definite (globally in the radius R)*
2. *V_{IO} is ∞ when $S_{vIO}(X) \rightarrow \infty$ (globally in the radius R)*
3. *If the system is globally stable, then $\dot{V}_{IO}$ is negative definite.*

Proof of Theorem 1: The Lyapunov function selected is given as follows:

$$V_{IO} = \frac{1}{2}S_{vIO}^2 \quad (16)$$

By combining Eq. (14), (15) with the first derivative of Eq. (16), and by choosing $k_v > \sigma_1$, the control law stabilizes the closed loop system of Eq. (3). Here σ_1 is already defined in (4). The first derivative of (16) is expressed as follows:

$$\dot{V}_{IO} = -k_v|S_{vIO}| + \sigma_1 S_{vIO} \quad (17)$$

When $k_v > \sigma_1$, then (17) is simplified based on the following conditions:

1. if $S_{vIO} > 0$, then $-k_v|S_{vIO}|$ is negative and $\sigma_1 S_{vIO}$ is positive, however the sum $-k_v|S_{vIO}| + \sigma_1 S_{vIO}$ is negative so $\dot{V}_{IO} \leq 0$

IEEE *Access*

N. Ullah *et al.*: Industrial Grade Adaptive Control Scheme for a Micro-Grid Integrated DAB Driven Battery Storage System
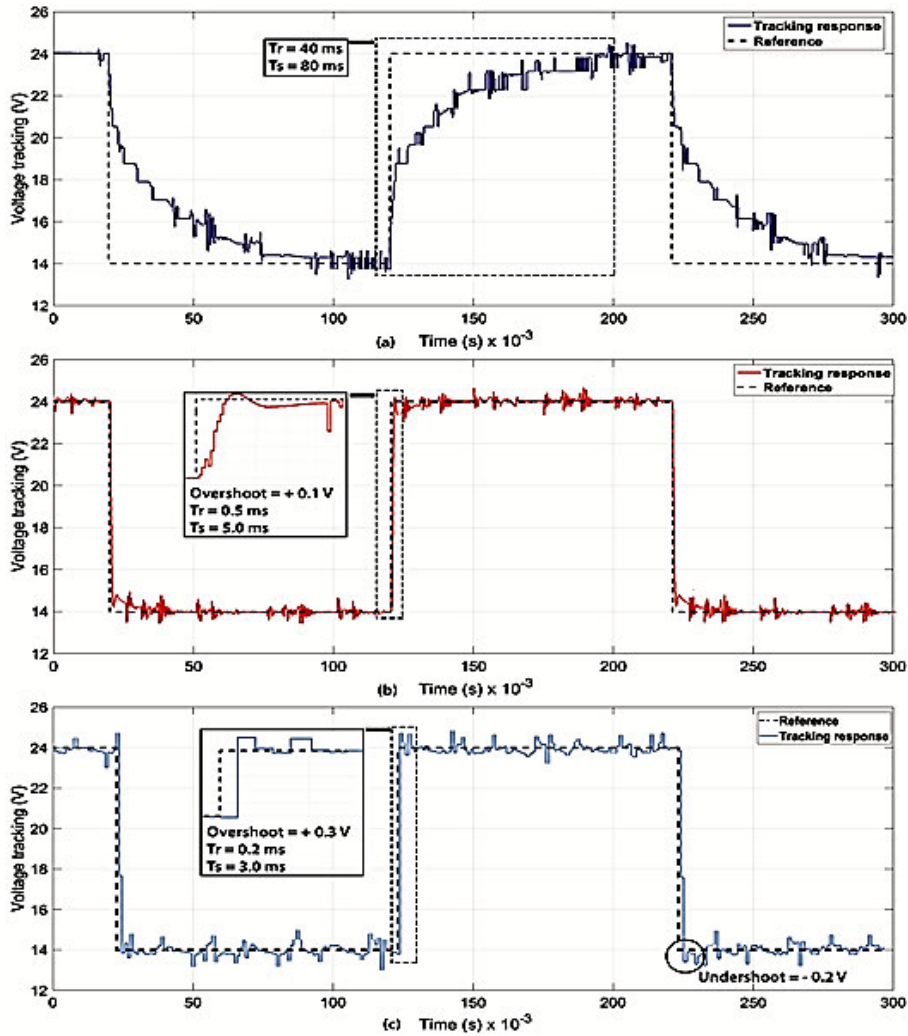
FIGURE 6. Performance comparison of controllers for varying voltage reference (a) Proportional Integral control paradigm (b) Proposed control paradigm (c) SMC control paradigm.
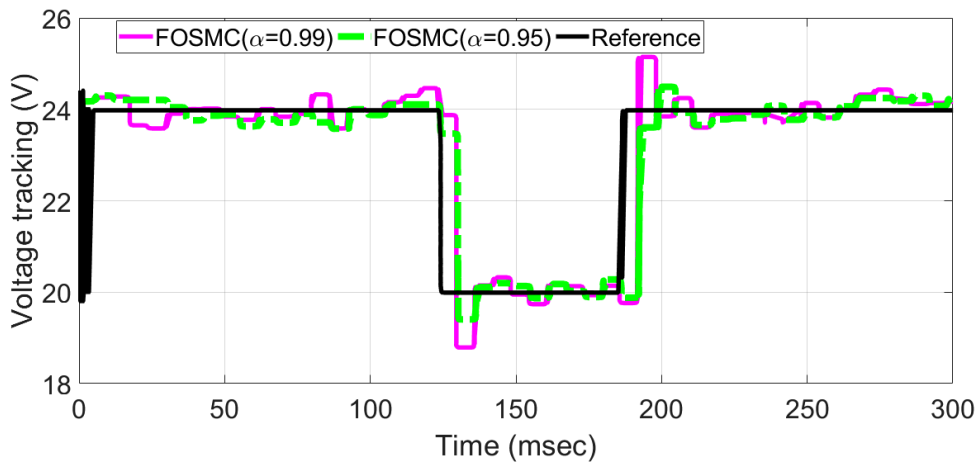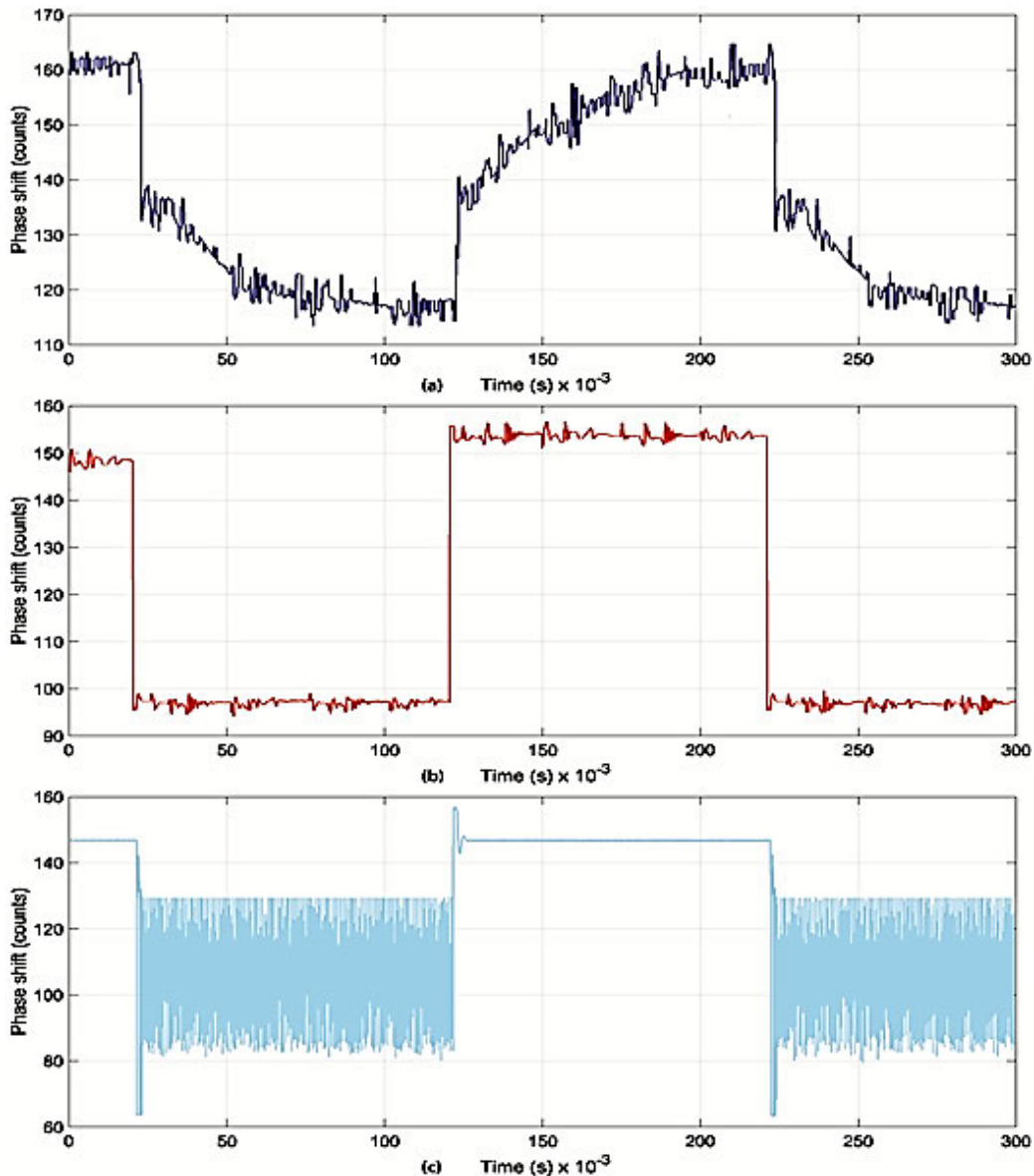

FIGURE 7. Performance comparison of controllers for varying voltage reference with FOSMC controllers with ($\alpha = 0.99$) and ($\alpha = 0.95$).

2. if $S_{vIO} < 0$, then $-k_v|S_{vIO}|$ is negative and $\sigma_1 S_{vIO}$ is also negative, so the sum $-k_v|S_{vIO}| + \sigma_1 S_{vIO}$ is also negative so $\dot{V}_{IO} \leq 0$. This proves Theorem 1.

C. FRACTIONAL ORDER SLIDING MODE CONTROL

In this subsection FOSMC system is derived for the voltage tracking problem of DIBMS system. Before deriving the

N. Ullah *et al.*: Industrial Grade Adaptive Control Scheme for a Micro-Grid Integrated DAB Driven Battery Storage System

IEEE *Access*

FIGURE 8. Phase shift for vaying reference (a) PI control scheme (b) Proposed control scheme (c)SMC control paradigm.

control system, the preliminaries of fractional calculus are mandatory to be understood, thus the basic definitions of fractional calculus are presented in Appendix-1. A fractional order sliding surface is defined as follows:

$$S_{vFO} = C_3 D^{-\alpha} e + C_4 \int \dot{e} \qquad (18)$$

where e is already defined in (5). Moreover C_3 and C_3 represent sliding surface constants. Apply the fractional operator D^α to (18), one obtains the following expression:

$$D^\alpha S_{vFO} = C_3 e + C_4 D^{\alpha-1} \dot{e} \qquad (19)$$

where $\dot{e} = \dot{X} - \dot{X}_d$. By combining (3) and (19), one obtains the following expression:

$$D^\alpha S_{vFO} = C_3 e + C_4 D^{\alpha-1}[A(X) + B(X)U + G(t) - \dot{X}_d] \qquad (20)$$

The control law is derived from (20) and expressed as follows:

$$U = (C_4 B(X))^{-1}[-C_4 A(X) + C_4 \dot{X}_d - C_3 D^{1-\alpha} e \\ - k_{v1} D^{1-\alpha} sgn(S_{vFO})] \qquad (21)$$

where k_{v1} represents the switching gain of the FOC paradigm. consider Theorem 2 given below.

Theorem 2: There exists a scalar function V_{FO} with continuous first derivative such that [53]:

1. V_{FO} *is positive definite (globally in the radius R)*
2. V_{FO} *is ∞ when $S_{vIO}(X) \to \infty$ (globally in the radius R)*
3. *If the system is globally stable, then $D_\alpha V_{FO}$ is negative definite and system states converge to the equilibrium points in finite time.*
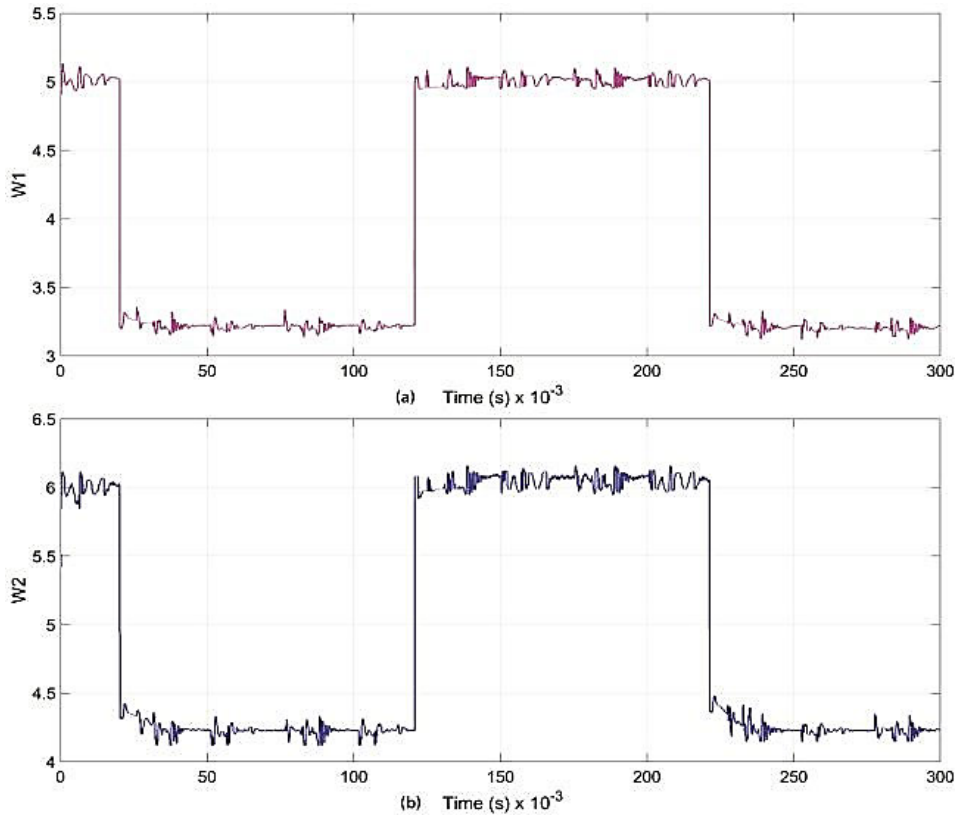
IEEE *Access*

N. Ullah *et al.*: Industrial Grade Adaptive Control Scheme for a Micro-Grid Integrated DAB Driven Battery Storage System

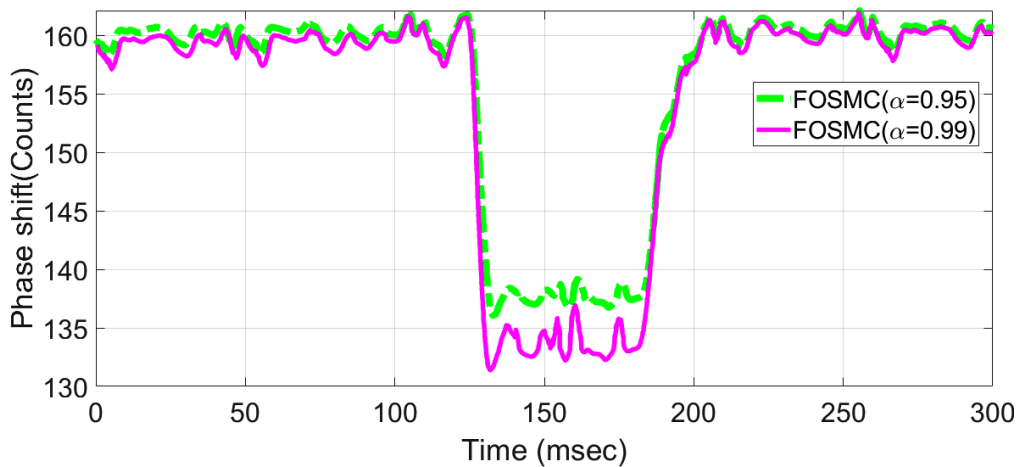**FIGURE 9.** Adaptive weight tuning (a) W_1 (b) W_2.

FIGURE 10. Phase shift for varying reference with FOSMC ($\alpha = 0.99$) and ($\alpha = 0.95$) controllers.

Proof of Theorem 2: In order to prove Theorem 2, the following inequality hold true [53]:

$$\left| \sum_{j=1}^{\infty} \frac{\Gamma(1+\alpha)}{\Gamma(1-j+\alpha)\Gamma(1+j)} D^j S_{vFO} D^{\alpha-j} S_{vFO} \right| \leq \Omega_1(S_{vFO}) \quad (22)$$

The Lyapunov candidate function is defined as follows:
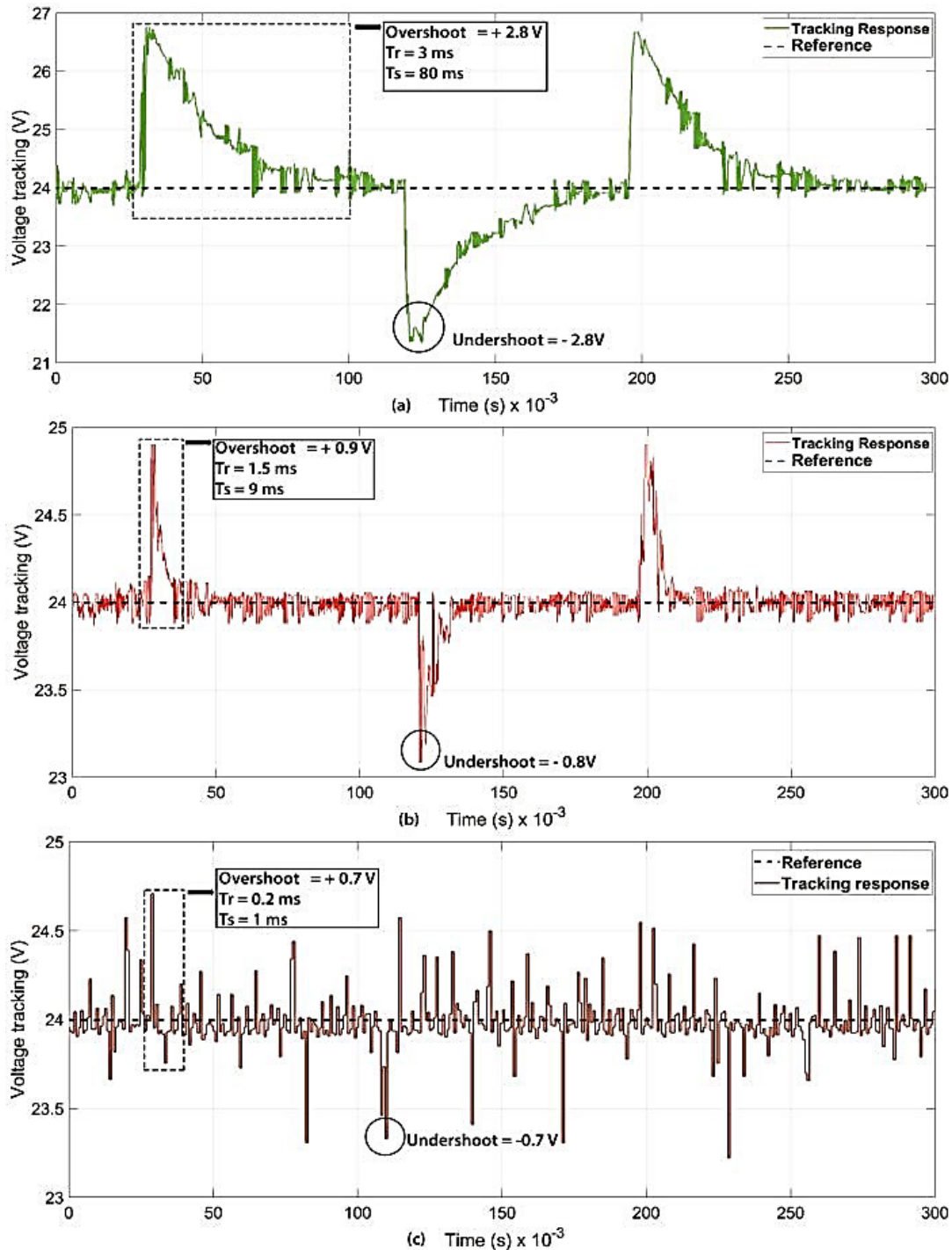
$$V_{FO} = \frac{1}{2} S_{vFO}^2 \quad (23)$$

Applying D^α to (23) yields the following expression [53]:

$$D^\alpha V_{FO}$$
$$\leq S_{vFO} D^\alpha S_{vFO}$$
$$+ \left| \sum_{j=1}^{\infty} \frac{\Gamma(1+\alpha)}{\Gamma(1-j+\alpha)\Gamma(1+j)} D^j S_{vFO} D^{\alpha-j} S_{vFO} \right| \quad (24)$$

Using assumption 1-2 and Eqs. 20-24, the following expression is obtained:

$$D^\alpha V_{FO} \leq -k_{v1}|S_{vFO}| + \sigma_1 S_{vFO} + \chi_1 \quad (25)$$

N. Ullah *et al.*: Industrial Grade Adaptive Control Scheme for a Micro-Grid Integrated DAB Driven Battery Storage System

IEEE *Access*

FIGURE 11. Performance comparison of controllers for varying source voltage (a) PI control scheme (b) Proposed control scheme (c) SMC Scheme.

By letting $k_{v1} > [\sigma_1, \chi_1]$, it can be easily shown that $D^\alpha V_{FO} \leq 0$ which means that the sliding surface reaching condition is satisfied and $S_{vFO} = 0$. This proves first part of Theorem 2. For the second part of Theorem 2, the derivation of the convergence proof is given in Appendix-2. From Appendix 2, (36) proves the finite time convergence of the state:

V. IMPLEMENTATION OF CONTROL SCHEMES

In order to implement the derived controllers, it is necessary to represent each controller as phase shift represented below:

$$U = cos\,(n - \varphi_z\,(n)) \qquad (26)$$
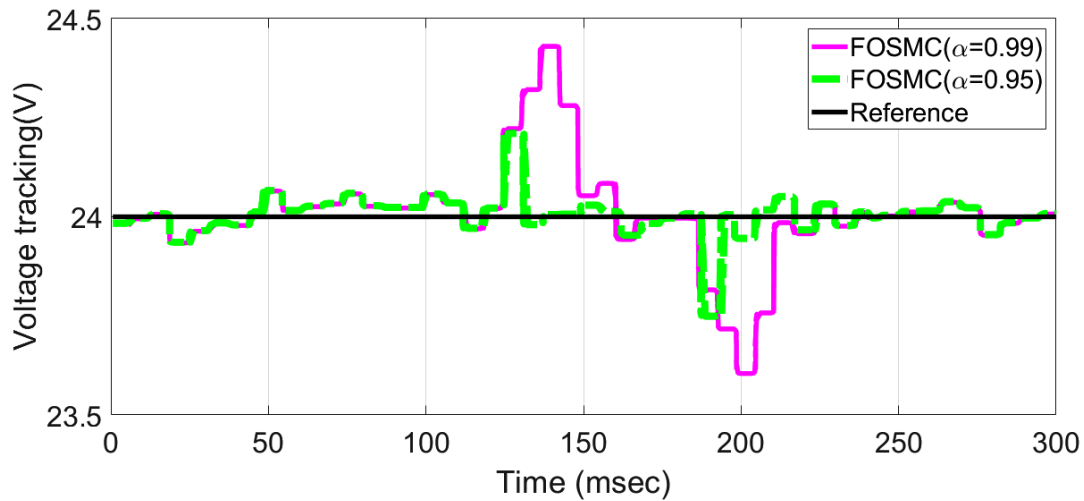
FIGURE 12. Voltage tracking performance under variable source voltage (a) FOSMC controllers with ($\alpha = 0.99$) and ($\alpha = 0.95$).

Therefore by using basic trigonometric laws, (26) can be expressed as follows:

$$\delta = \sin^{-1}(U) \qquad (27)$$

where δ represents the phase shift between the LV and HV bridges of the DIBMS converter. Moreover in order to implement the FOSMC scheme, it is necessary to implement fractional operators. Fig. 3 shows the implementation details of the fractional operator using DSP control card.

VI. RESULTS AND DISCUSSION

The experimental testing of the proposed control system using hardware in the loop (HIL) and processor in the loop (PIL) methods. HIL method is used for the verification of the controller robustness and PIL is used to calculate the CPU loading and time profiling of the control schemes. Parameters of the system and control schemes are tabulated in table 1 and 2.

A. ROBUSTNESS TEST: HARDWARE IN THE LOOP TESTING
Block diagram of the experiment is shown in Fig. 4. Also the experimental test bench is shown in Fig. 5.
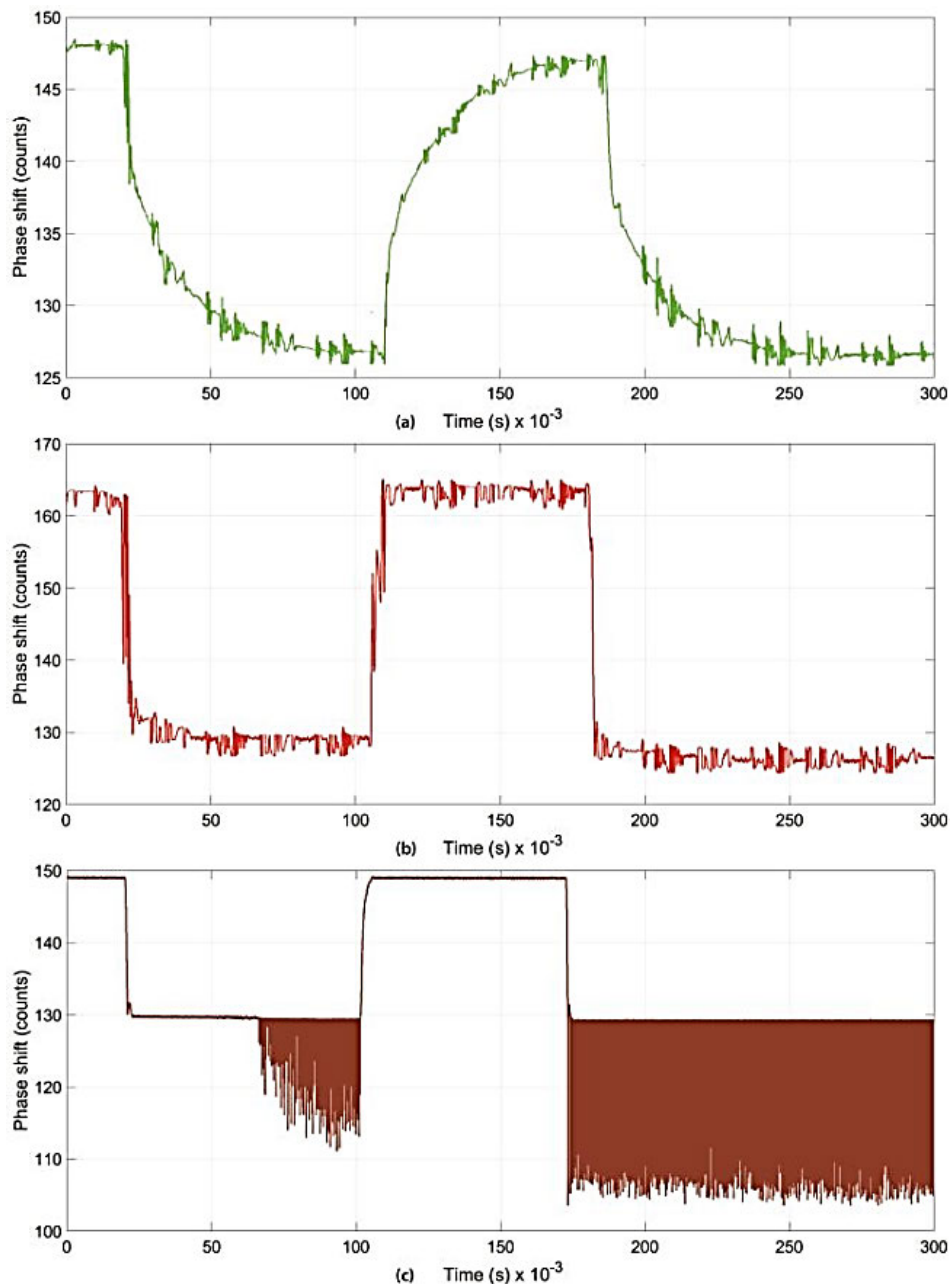
As shown in Fig. 4, the DIBMS system is integrated to a DC supply which emulates DC bus voltage. DAB is used to charge a battery bank of 24 Volts. DSP control card TMS320F28379D drives the power switches of the DAB converter through driving circuits. Moreover the control card communicates with MATLAB/Simulink environment in real time using high speed serial communication channel.

B. COMPUTATIONAL RESOURCE UTILIZATION TEST: PROCESSOR IN THE LOOP TESTING
In order to compute the utilized computational resources by each variant of controllers, a PIL test is conducted. Block diagram of the PIL test is shown in Fig. 16.

1) ROBUSTNESS TEST UNDER VARIABLE REFERENCE COMMAND
A variable reference voltage is applied to validate the DAB performance with PI, SMC and proposed control schemes. The resulted tracking response of the DAB with the various control paradigms is shown in Fig. 6. Initially a reference voltage of 24 V is used, that is abruptly changed to 14 V after $t = 20ms$. Another abrupt change is made to bring the reference signal again to 24 V after 100 ms of time at $t = 120ms$ and then again to 14 V after duration of 100 ms at $t = 220ms$. The PI response is slow and converges to reference voltage in 80 ms, whereas the rise time (T_r) for PI control paradigm is 40ms with no overshoot. Conversely, the proposed and SMC controllers have improved performance as compared to PI control scheme paradigm as shown in Fig. 6(b) and Fig. 6 (c) respectively. It can be seen from Fig. 6(c), that the compared to PI, SMC provides a minor overshoot of 0.3 V, rise time of 0.2 ms and the settling time is 3 ms. The proposed control scheme surpasses both the PI and SMC in terms of overshoot, rise time, and settling time as shown in Fig. 6(b). The proposed control is robust with fast convergence providing a more minor overshoot of $0.1v$ with rise time of 0.5 ms and settling time of 5 ms. The performance of FOSMC controller is validated using a reference voltage varying between 24 V and 20 V. The outturned response of FOSMC is shown in Fig. 7. Fig. 7 shows the FOSMC response for two different values of α. It can be seen that for $\alpha = 0.95$, the FOSMC has overshoot of $0.5v$ and undershoot of $-0.5v$, whereas for $\alpha = 0.99$, the FOSMC provided a higher overshoot of $1.1v$ and undershoot of $-1.1v$. Thus it is clear, that the FOSMC with $\alpha = 0.95$ has improved performance as compared to FOSMC with $\alpha = 0.99$. The corresponding phase shift counts generated with PI, proposed control scheme and SMC controllers is shown in Fig. 8. The PWM register counts are considered as phase shifts

N. Ullah *et al.*: Industrial Grade Adaptive Control Scheme for a Micro-Grid Integrated DAB Driven Battery Storage System

IEEE *Access*

FIGURE 13. Phase shift under source voltage variation (a) PI controller (b) Proposed controller (c) SMC controller.

ranging from 0 to 250 and corresponding to 0 and 90 degrees. As evident from Fig. 8a, the corresponding phase generated with PI controller does not settle in finite time, while in case of proposed control, it settles in finite time (Fig. 8b). For SMC controller, the phase shift count contains high frequency chattering (Fig. 8c) which is undesirable for practical implementations. The proposed controller utilizes adaptive Hebbian algorithm to tune its weight online. The corresponding experimental results are shown in Fig. 9. It is evident from the presented results, that the adaptive weights are adjusted subject to the change in reference command within the same time

interval, thus making proposed controller robust to changes. From the presented results and analysis, it is concluded that proposed controller is as robust as SMC and the phase count corresponding to proposed control is free of chattering. The corresponding phase shifts of the two variants of FOSMC schemes with source voltage variations are shown in Fig. 10. During $(125 \rightarrow 220)$ *ms* duration, whereas the reference voltage is abruptly changed from 24v to 20v, the resulting phase shifts show a decrements to lower values and at $t = 200$ *msec*, it increases and again becomes constant. For both variants of FOSMC, the phase shift count is initially fixed at

IEEE *Access*

N. Ullah *et al.*: Industrial Grade Adaptive Control Scheme for a Micro-Grid Integrated DAB Driven Battery Storage System
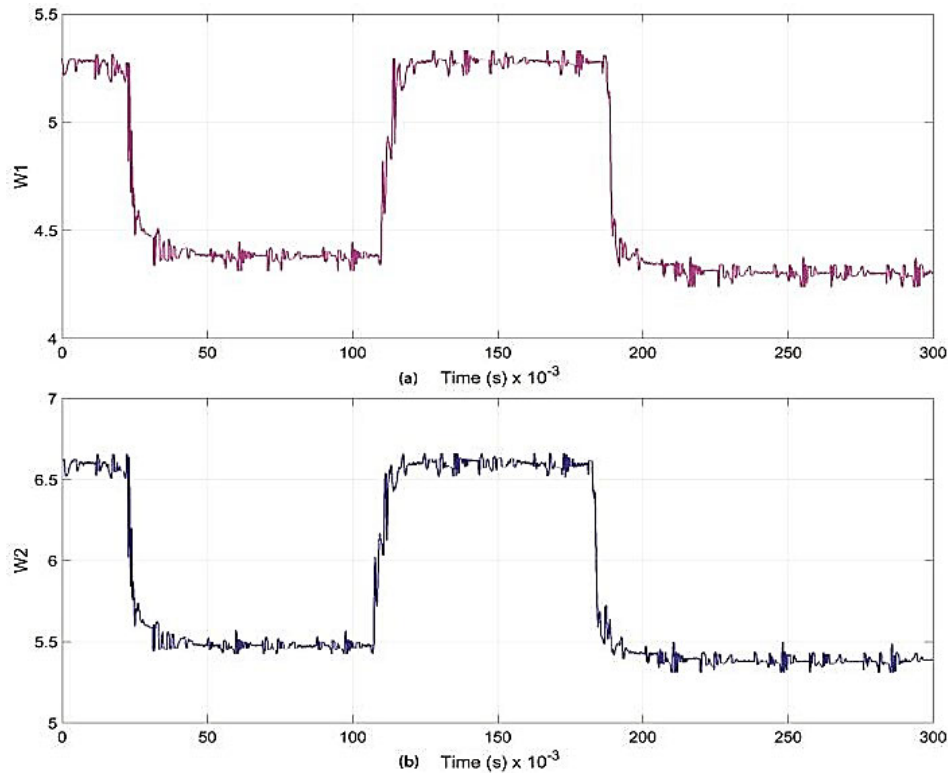

FIGURE 14. Adaptive weights tuning under source voltage variation (a) W_1 (b) W_2.

approximately 160 counts. In case of $\alpha = 0.99$, the phase shift counts decrements from 160 to 136 whereas in case of $\alpha = 0.95$, the noted decrements is from 160 to 132 respectively.

2) ROBUSTNESS TEST UNDER SOURCE VARIATION

In this test the reference voltage is kept constant whereas the source voltage is varied between $12V$ and $16V$. Initially, the source voltage is kept constant at $12V$ up to $t = 20ms$, and is then changed to $16V$ after $t = 20ms$ up to $t = 120ms$. The response of the PI, SMC, and proposed control schemes is shown in Fig. 11. The PI control paradigm shows a huge overshoot of $2.8V$ and also an undershoot of $-2.8V$ with slow convergence to the reference voltage as shown in Fig. 11 (a). The proposed control paradigm gives a better response as compared to PI control scheme with overshoot and undershoot of 0.9 V and $-0.8V$ respectively as shown in Fig. 11 (b). The SMC has much improved performance as compared to the PI and comparable performance as of the proposed control. SMC gives a lesser overshoot of 0.7 V and undershoot of -0.7 V as shown in Fig. 11(c). But, due to the inherent chattering phenomenon, the SMC is exposed to high frequency oscillations, questioning the practical viability of SMC paradigm.

To test FOSMC paradigm, the source voltage is varied between $12V \rightarrow 16V$ whereas the reference voltage is kept constant at 24 V. Initially, the input source voltage is kept

fixed at $12v$ from t$=(0 \rightarrow 120)$ *msec* and t$=(220 \rightarrow 300)$ *msec* and changing abruptly to $16v$ for t$=(120 \rightarrow 220)$ *msec*. Fig. 12 shows the resulting voltage response of the FOSMC paradigms for $\alpha = 0.95$ and $\alpha = 0.99$. The FOSMC scheme with $\alpha = 0.95$ converges at t $= 140$msec with overshoot of 0.2 V and undershoot of -0.2 V. Conversely, the FOSMC scheme converges at t $= 170$ *msec* with overshoot and undershoot of 0.2 V and -0.2 V respectively. This shows that the FOSMC scheme with $\alpha = 0.95$ has improved performance as compared to $\alpha = 0.99$.

Fig. 13 shows the corresponding phase shift counts generated with PI, proposed and SMC controllers. As evident from Fig. 13a, the corresponding phase generated with PI controller does not settle in finite time, while in case of proposed controller, it settles in finite time (Fig. 13b). For SMC controller, the phase shift count contains high frequency chattering (Fig. 13c) which is an undesirable phenomena for practical implementations. The proposed controller utilizes adaptive Hebbian algorithm to tune its weight online. The corresponding experimental results are shown in Fig. 14. It is evident from the presented results, that the adaptive weights are adjusted subject to the change in source voltage variations within the same time interval, thus making the proposed controller robust. Moreover the control signal is chatter free so making it feasible for practical implementations. The corresponding phase shifts for FOSMC are shown in Fig. 15. During the time $(125 \rightarrow 250)$ *msec*, when the source voltage
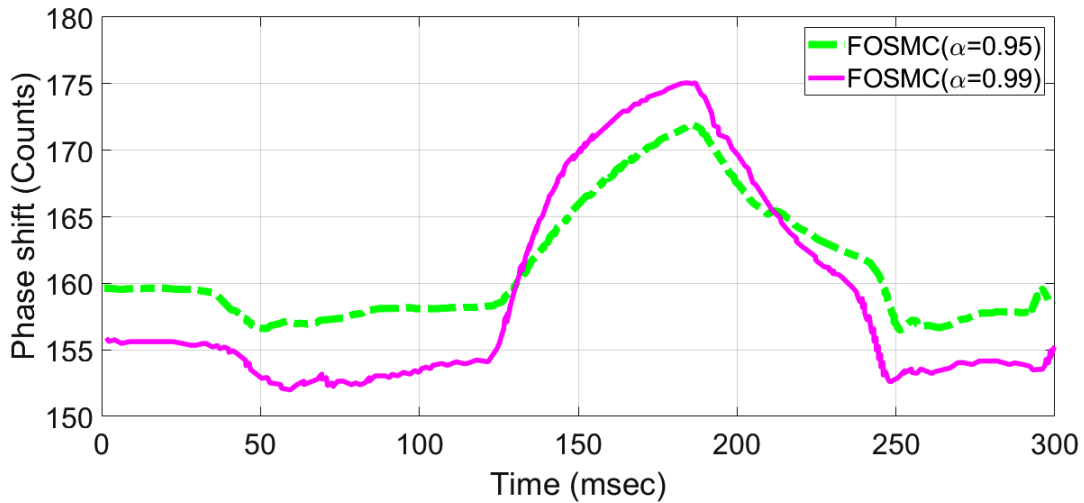
N. Ullah *et al.*: Industrial Grade Adaptive Control Scheme for a Micro-Grid Integrated DAB Driven Battery Storage System

IEEE *Access*

FIGURE 15. Phase shift under variable source voltage with FOSMC controller ($\alpha = 0.99$) and ($\alpha = 0.95$).

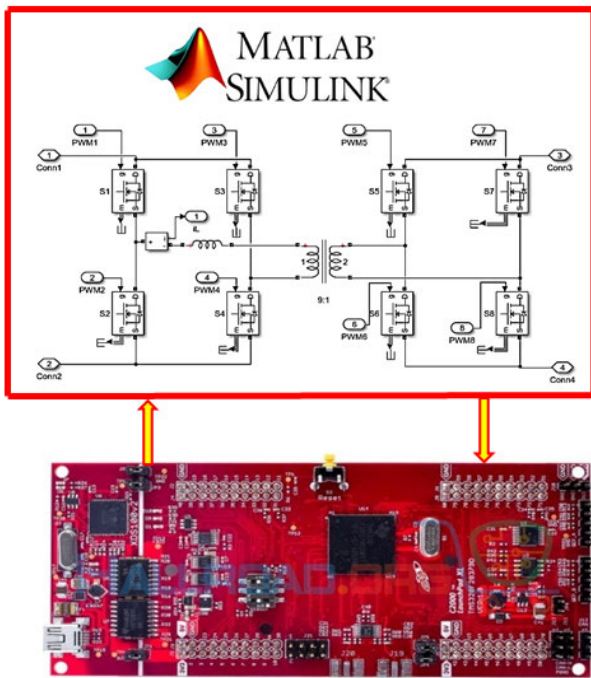**FIGURE 16.** Block diagram of PIL testing.

FIGURE 17. CPU loading.

the appropriate control signals and these are communicated through high speed serial port with the DAB converter running in the Simulink environment.

3) COMPARISON OF COMPUTATIONAL RESOURCE UTILIZATION AND TIME PROFILING

Fig. 17 shows the CPU utilization comparison of all variants of control schemes tested in this paper. A discrete version of PI control scheme utilizes small computational resources and CPU is loaded only by 2.11 %. The proposed control scheme is tested in PIL experiment and it utilizes medium computational resources and the CPU is loaded only by 12.43 %. Similarly, the PIL test results with integer order SMC control shows CPU loading of 19.02%. In the last test the FOSMC controller showed CPU loading of 29.28 %. Similarly the time profiling comparison of all variants of control schemes

is varied, an incremental variation in the the corresponding phase shifts for both variants of FOSMC is noted and again decreases to reach the constant settled count at $t = 250msec$. An incremental increase in the phase shift from 158 to 176 is noted for the FOSMC with $\alpha = 0.99$, whereas the incremental increase is from 160 to 172 for $\alpha = 0.95$.

In the PIL setup, DAB converter system runs in the software environment (Simulink), while the control system runs from the DSP hardware. DSP hardware generates
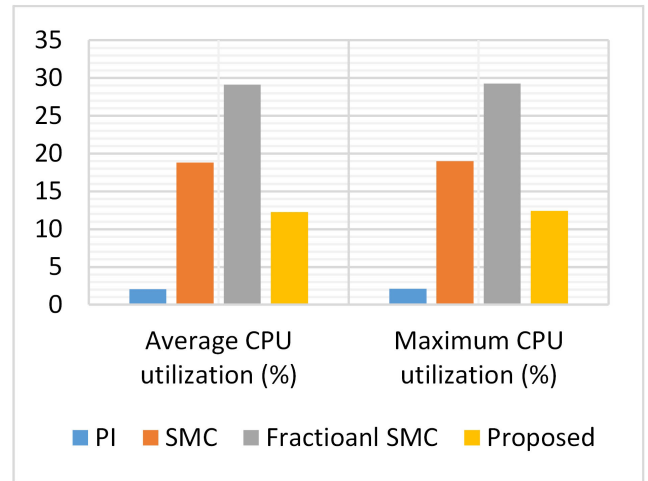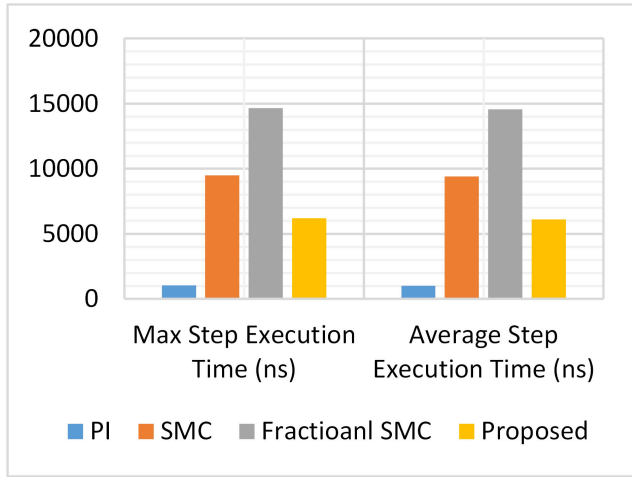
FIGURE 18. Time profiling comparison.

under test are shown in Fig. 18. The proposed controller utilized medium time profiling as compared to the SMC and FOSMC.

VII. CONCLUSION

In order to draw a meaningful conclusion about the research findings presented in this paper, 4 variants of control schemes have been derived and tested experimentally for a DIBMS system connected to a micro-grid system. As mentioned the goal of this paper was to find the best industrial grade controller which exhibits robustness and it also utilizes low computation resources. From The experimental results discussed above, the proposed control scheme is found to be as robust as SMC and FOSMC controllers. Moreover, the SMC control scheme offers high frequency chattering in control signal. With respect to the utilization of computational resources, FOSMC controller was the most expensive control scheme and CPU loading of 29.28 % was observed, followed by SMC controller with a loading of 19.02%, however it also introduced high frequency chatting in the control signal. PI controller utilized lesser resources of 2.11 % as compared to all other variants of control schemes however the control performance indicators are poor as evident from the presented results. The proposed controller caused a CPU loading of 12.43 % and its control performance indicators are as good as the robust control schemes such as SMC and the presented two variants of FOSMC. Thus, based on the collected results, the proposed controller turned out to be the best industrial controller for DIBMS integrated micro-gird system.

APPENDIX I

The fractional order operator mathematics are explained in this section under two definitions knows as Riemann–Liouville and Caputo fractional order derivatives and integrations. These both equations are differed by their dealing with initial conditions explained as follows:

The Riemann–Liouville Definition 1: According to this definition, the derivative and integration of a function $f(t)$ defined as follows [53].

$$_{t_0}I_t^\alpha f(t) = D_t^{-\alpha}f(t) = \frac{1}{\Gamma(\alpha)}\int_{t_0}^t \frac{f(\tau)}{(t-\tau)^{1-\alpha}}d\tau \tag{28}$$

$$_{t_0}D_t^\alpha f(t) = \frac{d^\alpha}{dt^\alpha}f(t) = \frac{1}{\Gamma(m-\alpha)}\frac{d^m}{dt^m}\int_{t_0}^t \frac{f(\tau)}{(t-\tau)^{\alpha-m+1}}d\tau \tag{29}$$

where $\Gamma(.)$ is the gamma function, $m \in N$ and $m - 1 < \alpha \leq m$

The following relation holds: $_{t_0}D_t^\alpha(_{t_0}I_t^\alpha f(t)) = f(t)$

The Caputo Fractional Order Derivative Definition 2: According to this definition, the derivative of a function $f(t)$ can be derived as follows [53]:

$$_{t_0}D_t^\alpha f(t)$$
$$= \begin{cases} \frac{1}{\Gamma(m-\alpha)}\int_{t_0}^t \frac{f^{(m)}(\tau)}{(t-\tau)^{\alpha-m+1}}d\tau; & m-1 < \alpha < m \\ \frac{d^m}{dt^m}f(t), & \alpha = m \end{cases} \tag{30}$$

The Caputo definitions can also be proven true for the following relation: $_{t_0}D_t^\alpha(_{t_0}I_t^\alpha f(t)) = f(t)$.

APPENDIX II

it has been proven from (25) that $S_{vFO} = 0$. Thus the (18) is expressed as follows:

$$e = -\frac{C_3}{C_4}D^{-\alpha}e \tag{31}$$

Lemma 1:. The following expression gives the fractional integral of function $f(t)$ with fractional derivative and is expressed as follows [53]:

$$_aD_t^{-\alpha} {}_aD_t^\alpha f(t) = f(t) - \sum_n^m [_aD_t^{\alpha-n}f(t)]_{t=a}\frac{[t-a]^{\alpha-n}}{\Gamma[\alpha-n+1]} \tag{32}$$

where Γ represents gamma function.

Lemma 2:. The following condition becomes true when the function $f(t)$ fraction integral is upper bounded [53]:

$$||_aD_t^{-\alpha}f(t)||_\rho \leq \psi_J||f(t)||_\rho; [1 \leq \psi_J \leq \infty; 1 \leq \rho \leq \infty] \tag{33}$$

Applying *Lemma 1* to the *LHS* expression of (31) and *Lemma 2* to the *RHS* of (31), one gets the following relation:

$$D^{-\alpha}D^\alpha e = e - [_{t_r}D_t^{\alpha-1}e]_{t=t_r}\frac{(t-t_r)^{\alpha-1}}{\Gamma(\alpha)} \tag{34}$$

From (34), when $t = t_r$ then $D^{-\alpha}D^\alpha e = e$. The expression $e = D^{-2}D^2 e$ is also mathematically valid. Applying *Lemma 1* to (34) one gets:.

$$D^{-2}D^2 e = e(t) - [_{t_r}D_t^{2-1}e]_{t=t_r}\frac{(t-t_r)^{2-1}}{2} - e(t_r) \tag{35}$$

N. Ullah *et al.*: Industrial Grade Adaptive Control Scheme for a Micro-Grid Integrated DAB Driven Battery Storage System

IEEE *Access*

Now applying the *Lemma 2* to the *RHS* terms of (31) gives the relation as follows:

$$|| - \frac{C_3}{C_4} D^{-\alpha} e|| - \leq \psi_J ||e||_\rho \quad (36)$$

Following expression is obtained when left hand side terms of (35) and (36) are combined:

$$||e(t) - [_{t_r} D_t^{2-1} e]_{t=t_r} \frac{(t - t_r)^{2-1}}{2}|| - ||e(t_r)|| \leq -\psi_J ||e||_\rho \quad (37)$$

The error $e(t)$ becomes zero by setting $t = t_s$ in (37) and the resulting remaining expression is given as follows:

$$t_r \leq t_s - \frac{2e(t_r)}{\dot{e}(t_r)} \quad (38)$$

Equation (38) validates the finite convergence time of the proposed controller.

REFERENCES

[1] A. Ipakchi and F. Albuyeh, "Grid of the future," *IEEE Power Energy Mag.*, vol. 7, no. 2, pp. 52–62, Mar./Apr. 2009.

[2] K. Sha, N. Alatrash, and Z. Wang, "A secure and efficient framework to read isolated smart grid devices," *IEEE Trans. Smart Grid*, vol. 8, no. 6, pp. 2519–2531, Nov. 2017.

[3] C. M. Martinez, X. Hu, D. Cao, E. Velenis, B. Gao, and M. Wellers, "Energy management in plug-in hybrid electric vehicles: Recent progress and a connected vehicles perspective," *IEEE Trans. Veh. Technol.*, vol. 66, no. 6, pp. 4534–4549, Jun. 2017.

[4] Z. Liu, D. Wang, H. Jia, N. Djilali, and W. Zhang, "Aggregation and bidirectional charging power control of plug-in hybrid electric vehicles: Generation system adequacy analysis," *IEEE Trans. Sustain. Energy*, vol. 6, no. 2, pp. 325–335, Apr. 2015.

[5] R. W. A. A. De Doncker, D. M. Divan, and M. H. Kheraluwala, "A three-phase soft-switched high-power-density DC/DC converter for high-power applications," *IEEE Trans. Ind. Appl.*, vol. 27, no. 1, pp. 63–73, Jan. 1991.

[6] K. Wang, F. C. Lee, and J. Lai, "Operation principles of bi-directional full-bridge DC/DC converter with unified soft-switching scheme and soft-starting capability," in *Proc. 15th Annu. IEEE Appl. Power Electron. Conf. Expo. (APEC)*, New Orleans, LA, USA, Feb. 2000, pp. 111–118.

[7] J.-W. Yang and H.-L. Do, "Soft-switching dual-flyback DC–DC converter with improved efficiency and reduced output ripple current," *IEEE Trans. Ind. Electron.*, vol. 64, no. 5, pp. 3587–3594, May 2017.

[8] D. Murthy-Bellur and M. K. Kazimierczuk, "Isolated two-transistor zeta converter with reduced transistor voltage stress," *IEEE Trans. Circuits Syst. I, Reg. Papers*, vol. 58, no. 1, pp. 41–45, Jan. 2011.

[9] F. Zhang and Y. Yan, "Novel forward–flyback hybrid bidirectional DC–DC converter," *IEEE Trans. Ind. Electron.*, vol. 56, no. 5, pp. 1578–1584, May 2009.

[10] Z. Zhang, O. C. Thomsen, and M. A. E. Andersen, "Optimal design of a push-pull-forward half-bridge (PPFHB) bidirectional DC–DC converter with variable input voltage," *IEEE Trans. Ind. Electron.*, vol. 59, no. 7, p. 2761–2771, Jul. 2012.

[11] L. Roggia and P. F. S. Costa, "Comparative analysis between integrated full-bridge-forward and dual active bridge DC–DC converters," *Electron. Lett.*, vol. 54, no. 4, pp. 231–233, Feb. 2018.

[12] P. Xia, H. Shi, H. Wen, Q. Bu, Y. Hu, and Y. Yang, "Robust LMI-LQR control for dual-active-bridge DC–DC converters with high parameter uncertainties," *IEEE Trans. Transport. Electrific.*, vol. 6, no. 1, pp. 131–145, Mar. 2020.

[13] M. Phattanasak, W. Kaewmanee, P. Thounthong, P. Sethakul, J.-P. Martin, S. Pierfederici, and B. Davat, "Flatness based control of a dual active bridge converter for DC microgrid," in *Proc. 39th Annu. Conf. IEEE Ind. Electron. Soc. (IECON)*, Vienna, Austria, Nov. 2013, pp. 7926–7931.

[14] X. Fei, Z. Feng, N. PuQi, and W. Xuhui, "Analyzing ZVS soft switching using single phase shift control strategy of dual active bridge isolated DC-DC converters," in *Proc. 21st Int. Conf. Electr. Mach. Syst. (ICEMS)*, Jeju, Oct. 2018, pp. 2378–2381.

[15] F. Krismer and J. W. Kolar, "Accurate small-signal model for the digital control of an automotive bidirectional dual active bridge," *IEEE Trans. Power Electron.*, vol. 24, no. 12, pp. 2756–2768, Dec. 2009, doi: 10.1109/TPEL.2009.2027904.

[16] M. Hong, G. Xuanjie, Z. Chengbi, and D. Shujiang, "An improved dual phase shift control strategy for dual active bridge DC-DC converter with soft switching," in *Proc. Int. Power Electron. Conf. (IPEC-Niigata-ECCE Asia)*, Niigata, Japan, May 2018, pp. 2718–2724.

[17] S. Bal, D. B. Yelaverthi, A. K. Rathore, and D. Srinivasan, "Improved modulation strategy using dual phase shift modulation for active commutated current-fed dual active bridge," *IEEE Trans. Power Electron.*, vol. 33, no. 9, pp. 7359–7375, Sep. 2018, doi: 10.1109/TPEL.2017.2764917.

[18] J. Qiu, K. Shen, A. Tong, L. Hang, and J. Liao, "Unified ZVS strategy for DAB with triple-phase-shift modulation in boost mode," *J. Eng.*, vol. 2019, no. 18, pp. 4906–4910, Jul. 2019.

[19] H. Zhang, X. Tong, and J. Yin, "Optimal triple-phase-shift controller design of isolated bidirectional DC-DC converter based on ant colony algorithm and BP neural network," in *Proc. IECON 43rd Annu. Conf. IEEE Ind. Electron. Soc.*, Beijing, China, Oct. 2017, pp. 8802–8807.

[20] A. Burgio, D. Menniti, M. Motta, A. Pinnarelli, N. Sorrentino, and P. Vizza, "A laboratory model of a dual active bridge DC-DC converter for a smart user network," in *Proc. IEEE 15th Int. Conf. Environ. Electr. Eng. (EEEIC)*, Rome, Italy, Jun. 2015, pp. 997–1002, doi: 10.1109/EEEIC.2015.7165300.

[21] F. L. F. Marcelino, H. H. Sathler, T. R. de Oliveira, and P. F. Donoso-Garcia, "Modeling and control of a dual active bridge for energy storage in DC microgrid applications," in *Proc. IEEE 8th Int. Symp. Power Electron. for Distrib. Gener. Syst. (PEDG)*, Florianopolis, Brazil, Apr. 2017, pp. 1–8, doi: 10.1109/PEDG.2017.7972461.

[22] L. Xue, D. Diaz, Z. Shen, F. Luo, P. Mattavelli, and D. Boroyevich, "Dual active bridge based battery charger for plug-in hybrid electric vehicle with charging current containing low frequency ripple," in *Proc. 28th Annu. IEEE Appl. Power Electron. Conf. Expo. (APEC)*, Long Beach, CA, USA, Mar. 2013, pp. 1920–1925, doi: 10.1109/APEC.2013.6520557.

[23] S. Khade, A. Gaonkar, S. Weakey, R. Chavan, and R. Meshram, "Stability enhancement of rectifier and DAB stages of SST model using dynamic phasor based PI controller," in *Proc. IEEE 6th Int. Conf. Power Syst. (ICPS)*, New Delhi, India, Mar. 2016, pp. 1–6, doi: 10.1109/ICPES.2016.7584146.

[24] X. Lu, J. M. Guerrero, K. Sun, and J. C. Vasquez, "An improved droop control method for DC microgrids based on low bandwidth communication with DC bus voltage restoration and enhanced current sharing accuracy," *IEEE Trans. Power Electron.*, vol. 29, no. 4, pp. 1800–1812, Apr. 2014.

[25] C. Komathi and M. G. Umamaheswari, "Design of gray wolf optimizer algorithm-based fractional order PI controller for power factor correction in SMPS applications," *IEEE Trans. Power Electron.*, vol. 35, no. 2, pp. 2100–2118, Feb. 2020, doi: 10.1109/TPEL.2019.2920971.

[26] H. Qin and J. W. Kimball, "Closed-loop control of DC–DC dual-active-bridge converters driving single-phase inverters," *IEEE Trans. Power Electron.*, vol. 29, no. 2, pp. 1006–1017, Feb. 2014, doi: 10.1109/TPEL.2013.2257859.

[27] W. L. Malan, D. M. Vilathgamuwa, G. Walker, D. J. Thrimawithana, and U. K. Madawala, "Modeling and control of a CLC resonant dual active bridge," in *Proc. Australas. Universities Power Eng. Conf. (AUPEC)*, Perth, WA, Australia, Sep. 2014, pp. 1–6, doi: 10.1109/AUPEC.2014.6966537.

[28] G. G. Koch, S. S. Queiroz, C. Rech, R. C. L. F. Oliveira, R. A. Borges, E. S. Tognetti, and V. F. Montagner, "Design of a robust PI controller for a dual active bridge converter," in *Proc. 12th IEEE Int. Conf. Ind. Appl. (INDUSCON)*, Curitiba, Brazil, Nov. 2016, pp. 1–6, doi: 10.1109/INDUSCON.2016.7874503.

[29] F. Xiong, J. Wu, Z. Liu, and L. Hao, "Current sensorless control for dual active bridge DC–DC converter with estimated load-current feedforward," *IEEE Trans. Power Electron.*, vol. 33, no. 4, pp. 3552–3566, Apr. 2018, doi: 10.1109/TPEL.2017.2705344.

[30] Y. Jeung and D. Lee, "Sliding mode control of bi-directional dual active bridge DC/DC converters for battery energy storage systems," in *Proc. IEEE Appl. Power Electron. Conf. Expo. (APEC)*, Tampa, FL, USA, Mar. 2017, pp. 3385–3390, doi: 10.1109/APEC.2017.7931182.

[31] S. C. Tan, Y. M. Lai, and C. K. Tse, *Sliding Mode Control of Switching Power Converters: Techniques and Implementation*, vol. 12. Boca Raton, FL, USA: CRC Press, Dec. 2017, pp. 1–9.

[32] S. Talbi, A. M. Mabwe, and A. E. Hajjaji, "Control of a bidirectional dual active bridge converter for charge and discharge of a li-ion battery," in *Proc. IEEE IECON*, Nov. 2015, pp. 849–856.

[33] Z. Yu, J. Zeng, J. Liu, and F. Luo, "Terminal sliding mode control for dual active bridge DC-DC converter with structure of voltage and current double closed loop," in *Proc. Austral. New Zealand Control Conf. (ANZCC)*, Melbourne, VIC, Australia, Dec. 2018, pp. 11–15, doi: 10.1109/ANZCC.2018.8606608.

[34] K. Li, Y. Yang, S.-C. Tan, and R. S.-Y. Hui, "Sliding-mode-based direct power control of dual-active-bridge DC-DC converters," in *Proc. IEEE Appl. Power Electron. Conf. Expo. (APEC)*, Anaheim, CA, USA, Mar. 2019, pp. 188–192, doi: 10.1109/APEC.2019.8721849.

[35] I. Ruiz, E. Vidal-Idiarte, and J. Calvente, "Direct digital design of a proportional robust control based on sliding for dual active bridge converters," in *Proc. IECON 45th Annu. Conf. IEEE Ind. Electron. Soc.*, Lisbon, Portugal, Oct. 2019, pp. 1696–1701, doi: 10.1109/IECON.2019.8927512.

[36] C. Cecati, F. Ciancetta, and P. Siano, "A multilevel inverter for photovoltaic systems with fuzzy logic control," *IEEE Trans. Ind. Electron.*, vol. 57, no. 12, pp. 4115–4125, Dec. 2010, doi: 10.1109/TIE.2010.2044119.

[37] A. Bouafia, F. Krim, and J.-P. Gaubert, "Fuzzy-logic-based switching state selection for direct power control of three-phase PWM rectifier," *IEEE Trans. Ind. Electron.*, vol. 56, no. 6, pp. 1984–1992, Jun. 2009, doi: 10.1109/TIE.2009.2014746.

[38] S. Talbi, A. M. Mabwe, and A. El Hajjaji, "PI-fuzzy control of a bidirectional Dual Active Bridge converter," in *Proc. Amer. Control Conf. (ACC)*, Seattle, WA, USA, 2017, pp. 1271–1277, doi: 10.23919/ACC.2017.7963127.

[39] R. Zgheib and K. Al-Haddad, "Neural network controller to manage the power flow of a hybrid source for electric vehicles," in *Proc. IEEE Vehicle Power Propuls. Conf. (VPPC)*, Montreal, QC, USA, Oct. 2015, pp. 1–6.

[40] N. Ullah, M. Asghar, A. Khattak, and M. M. Rafiq, "Comparison of integer and fractional order robust controllers for DC/DC converter feeding constant power load in a DC microgrid," *Sustain. Energy, Grids Netw.*, vol. 12, pp. 1–9, Dec. 2017.

[41] I. Sami, S. Ullah, Z. Ali, N. Ullah, and J.-S. Ro, "A super twisting fractional order terminal sliding mode control for DFIG-based wind energy conversion system," *Energies*, vol. 13, no. 9, p. 2158, May 2020.

[42] S.-W. Seo and H. H. Choi, "Digital implementation of fractional order PID-type controller for boost DC–DC converter," *IEEE Access*, vol. 7, pp. 142652–142662, 2019, doi: 10.1109/ACCESS.2019.2945065.

[43] S. Tang, Y. Sun, Y. Chen, Y. Zhao, Y. Yang, and W. Szeto, "An enhanced MPPT method combining fractional-order and fuzzy logic control," *IEEE J. Photovolt.*, vol. 7, no. 2, pp. 640–650, Mar. 2017, doi: 10.1109/JPHOTOV.2017.2649600.

[44] Z. Qi, J. Tang, J. Pei, and L. Shan, "Fractional controller design of a DC-DC converter for PEMFC," *IEEE Access*, vol. 8, pp. 120134–120144, 2020, doi: 10.1109/ACCESS.2020.3005439.

[45] C. Komathi and M. G. Umamaheswari, "Design of gray Wolf optimizer algorithm-based fractional order PI controller for power factor correction in SMPS applications," *IEEE Trans. Power Electron.*, vol. 35, no. 2, pp. 2100–2118, Feb. 2020, doi: 10.1109/TPEL.2019.2920971.

[46] A. B. Sharkawy, "A computationally efficient fuzzy control scheme for a class of MIMO systems," *Alexandria Eng. J.*, vol. 52, no. 4, pp. 583–594, Dec. 2013.

[47] M. Ahmeid, M. Armstrong, M. Al-Greer, and S. Gadoue, "Computationally efficient self-tuning controller for DC–DC switch mode power converters based on partial update Kalman filter," *IEEE Trans. Power Electron.*, vol. 33, no. 9, pp. 8081–8090, Sep. 2018.

[48] V. Duchaine, S. Bouchard, and C. M. Gosselin, "Computationally efficient predictive robot control," *IEEE/ASME Trans. Mechatronics*, vol. 12, no. 5, pp. 570–578, Oct. 2007, doi: 10.1109/TMECH.2007.905722.

[49] M. Easley, S. Jain, M. B. Shadmand, and H. Abu-Rub, "Computationally efficient distributed predictive controller for cascaded multilevel impedance source inverter with LVRT capability," *IEEE Access*, vol. 7, pp. 35731–35742, 2019, doi: 10.1109/ACCESS.2019.2904392.

[50] N. Ullah, A. Ullah, A. Ibeas, and J. Herrera, "Improving the hardware complexity by exploiting the reduced dynamics-based fractional order systems," *IEEE Access*, vol. 5, pp. 7714–7723, 2017, doi: 10.1109/ACCESS.2017.2700439.

[51] Z. Farooq, T. Zaman, M. A. Khan, Nasimullah, S. M. Muyeen, and A. Ibeas, "Artificial neural network based adaptive control of single phase dual active bridge with finite time disturbance compensation," *IEEE Access*, vol. 7, pp. 112229–112239, 2019, doi: 10.1109/ACCESS.2019.2934253.

[52] J. J. E. Slotine and W. Li, *Applied Nonlinear Control*, vol. 199. Englewood Cliffs, NJ, USA: Prentice-Hall, 1991.

[53] M. O. Efe, "Fractional fuzzy adaptive sliding-mode control of a 2-DOF direct-drive robot arm," *IEEE Trans. Syst., Man, Cybern. B, Cybern.*, vol. 38, no. 6, pp. 1561–1570, Dec. 2008, doi: 10.1109/TSMCB.2008.928227.

NASIM ULLAH received the Ph.D. degree in mechatronic engineering from Beihang University, Beijing, China, in 2013. From September 2006 to 2010, he was a Senior Design Engineer with IICS, Pakistan. He is currently working as an Associate Professor of electrical engineering with Taif University, Saudi Arabia. His research interests include renewable energy, flight control systems, integer and fractional order modeling of dynamic systems, integer/fractional order adaptive robust control methods, fuzzy/NN, hydraulic and electrical servos, epidemic, and vaccination control strategies.

ZAHEER FAROOQ received the B.Sc. and M.Sc. degrees in electrical engineering from the University of Science and Technology, Peshawar, Pakistan, in 2003 and 2009, respectively. He is currently pursuing the Ph.D. degree with the CECOS University of IT and Emerging Sciences, Peshawar, Pakistan, where he is also an Assistant Professor. His current research interests include motor control and drives, renewable energy, and control of dc/dc power converters.

IRFAN SAMI received the B.Sc. degree in electrical engineering from the University of Engineering and Technology, Peshawar–Bannu, Pakistan, in 2016, and the M.Sc. degree in electrical engineering from COMSATS University Islamabad–Abbottabad, Abbottabad, Pakistan, in 2019. He is currently pursuing the Ph.D. degree in electrical engineering with Chung-Ang University, Seoul, South Korea. His research interests include electric drives, renewable energies, and electrical machine design.

N. Ullah *et al.*: Industrial Grade Adaptive Control Scheme for a Micro-Grid Integrated DAB Driven Battery Storage System

IEEE *Access*

MD. SHAHARIAR CHOWDHURY received the B.Sc. degree in engineering (EEE) from the Atish Dipankar University Science Technology, Bangladesh, in 2015, the M.Sc. degree from the Prince of Songkla University, Hat Yai, Thailand, in 2019, and the M.Sc. degree from Universiti Kebangsaan Malaysia (UKM), in 2019. He is currently working as a Research Fellow with the Prince of Songkla University. His research interests include renewable energy, solar PV, thin film, perovskite solar cells, solar PV waste recycling, and semiconductor materials. He has published a Review Article and a Research Article in the ISI index journal. His research area highlighted twice in the sustainable newspaper (Eco-Business.com). He is also an Editorial Member of the *International Journal of Sustainable and Renewable Energy*.

KUAANAN TECHATO received the B.Eng. (ME) degree from the Prince of Songkla University, Thailand, in 1995, the M.Eng. (IE) degree from Chulalongkorn University, in 1999, the M.Sc. (EBM) degree from Warwick University, in 1999, and the Ph.D. degree from Chulalongkorn University, in 2008. He is currently working as an Assistant Professor with the Prince of Songkla University, Hat Yai, Thailand, where he is also serving as the Dean for the Faculty of Environmental Management. His research interests include renewable energy, heat-pump, and power systems and control. He has been a Keynote Speaker and an Invited Speaker at many international conferences. He has published many technical articles to various journals and international conferences. He is also involved with many journals, as an editor or an associate editor, and a successful organizer of many international conferences.

HEND IBRAHEEM ALKHAMMASH received the M.Sc. and Ph.D. degrees in electronic and electrical engineering from the University of Southampton, U.K. She is currently an Assistant Professor with the Department of Electrical Engineering, College of Engineering, Taif University, Saudi Arabia. She is also a Vice-Dean of the University Development Deanship, Taif University. Her research interests include nanotechnology, renewable energy, and micro-fluid devices. She also works as an External Reviewer of the National Commission for Academic Accreditation and Assessment (NCAAA). She was awarded a Senior Fellow of the Higher Education Academy (SFHEA) in January 2020.

● ● ●